Springer

KSME

Journal of Mechanical Science and Technology 30 (4) (2016) 1603~1610
www.springerlink.com/content/1738-494x(Print)/1976-3824(Online)
DOI 10.1007/s12206-016-0315-2

Influence of tip clearance on pressure fluctuations in an axial flow pump †

Jianjun Feng*, Xingqi Luo, Pengcheng Guo and Guangkuan Wu

State Key Laboratory Base of Eco-Hydraulic Engineering in Arid Area, Xi'an University of Technology, Xi'an, 710048, China

(Manuscript Received May 27, 2015; Revised November 20, 2015; Accepted December 15, 2015)

Abstract

Rotor-stator interaction in axial pumps can produce pressure fluctuations and further vibrations even damage to the pump system in some extreme case. In this paper, the influence of tip clearance on pressure fluctuations in an axial flow water pump has been investigated by numerical method. Three-dimensional unsteady flow in the axial flow water pump has been simulated with different tip clearances between the impeller blade tip and the casing wall. In addition to monitoring pressure fluctuations at some typical points, a new method based on pressure statistics was proposed to determine pressure fluctuations at all grid nodes inside the whole pump. The comparison shows that the existence of impeller tip clearance magnifies the pressure fluctuations in the impeller region, from the hub to shroud. However, the effect on pressure fluctuation in the diffuser region is not evident. Furthermore, the tip clearance vortex has also been examined under different tip clearances.

Keywords: Axial-flow pump; Tip clearance; Computational fluid dynamics; Rotor-stator interaction; Pressure fluctuation

1. Introduction

Axial flow pumps are widely used in engineering due to the capacity of transporting a larger flow rate. The internal flow field of an axial flow pump is extremely complex and totally turbulent, including backward leakage flow, vortex shedding from the impeller blade tip, unsteady boundary layers on the blade and the adjacent casing, as well as the flow interaction between the main flow and the backward leakage flow through the impeller blade tip clearance driven by the pressure difference between the blade pressure side and suction side [1]. Furthermore, due to relative motion between the impeller and diffuser, as well as the inherent characteristic of high turbulence in the flow with a high Reynolds number, the pressure fluctuation in the pump is very strong, inducing vibrations and extra hydraulic forces to the pump components, together with some noise to the environment.

Many investigations including numerical simulations and experimental measurements have been carried out to capture flow structures in axial flow water pumps, mostly focusing on the flow structure of tip leakage vortex. Zierke et al. [2, 3] reported experiment results obtained from two-dimensional Laser Doppler velocimetry (LDV) and oil-paint method in the impeller tip clearance region, investigating the effects of tip clearance size on the structure of the rotor tip leakage vortex, as well as the trajectory of the tip leakage vortex core. Wu et al. [3] applied two-dimensional Particle image velocimetry (PIV) technique to measure the tip vortex flow structure in the meridonal plane of an axial flow pump, more attention was paid to the rollup and breakdown of the tip vortex. Zhang et al. [4, 5] conducted numerical simulations for an axial flow pump with four impeller blades and seven diffuser vanes using a commercial CFD code to study the tip leakage vortex structure and trajectory, and the results were compared with experimental images obtained with a high speed camera. They found that the starting point of tip leakage vortex occurs near the impeller blade leading edge at part-load conditions, and it moves from leading edge to about 30% chord length at the design flow rate.

Pressure fluctuation has been extensively investigated in radial pumps, including pressure fluctuations generated by impeller-tongue interactions [6-8] and also impeller-diffuser interactions [9-13]. However, the work related to pressure fluctuations in axial pumps is relatively scarce. Zhang et al. [14] utilized pressure transducers to study the pressure fluctuation in an axial flow pump. They demonstrated that pressure fluctuation amplitude increases from the hub to the tip in the impeller, the greatest pressure fluctuation occurs at the impeller inlet, and the blade passing frequency is dominant in the frequency spectrums. Shuai et al. [15] carried out numerical simulations in an axial-flow water pump to examine the pressure fluctuation characteristics at several typical monitor points. They pointed out that pressure fluctuation on the impeller blades decreases from hub to shroud and the presence of

*Corresponding author. Tel.: +86 29 82312910, Fax.: +86 29 82312857
E-mail address: jianjunfeng@xaut.edu.cn
† Recommended by Associate Editor Seongwon Kang

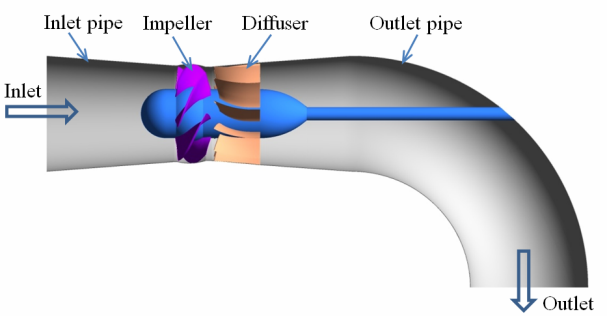

Fig. 1. Computational domain of the pump.

vortex structures has influences on the pressure fluctuation near the impeller outlet. Recently, Kang et al. [16] have examined the influence of stator vane number on the performance including pressure fluctuations of an axial-flow pump. Ji et al. [17] investigated the alleviation of pressure fluctuations around a marine propeller with different skew angles.

Due to limited research linked to pressure fluctuations in axial flow pumps, the understanding on generation mechanism and transportation characteristics of pressure fluctuation is still not satisfying. In particular, the influence of tip clearance on pressure fluctuation needs to be examined in detail. Furthermore, both numerical simulations and measurements on pressure fluctuations have been performed only on some selected monitoring points in CFD simulations or some limited measuring positions in experiments, thus resulting in possible neglecting of some important features due to the limited points of investigation. In this paper, the internal unsteady flow field in an axial flow pump has been numerically investigated, and the pressure fluctuation inside the whole pump has been calculated through a post-processing at all grid nodes. The standard deviation of unsteady pressure denotes the amount of pressure variation for a serial of fluctuating pressures. It is assumed to be more accurate to quantify the pressure fluctuation than the method of peak-to-peak difference of unsteady pressure, and is adopted in this paper. In addition, the influence of blade tip clearance on pressure fluctuation has been examined.

2. Numerical methodology

2.1 Geometry

The axial flow pump under investigation is shown in Fig. 1 in a three-dimensional view, with the complete hydraulic flow path taken as computational domains for CFD simulations. The outer diameter of the impeller blade is D_2 = 0.3 m, with a tip clearance of 0.3 mm to the impeller casing wall. The impeller has six three-dimensional blades, equipped with eleven two-dimensional vanes for the diffuser. The design rotating speed is n = 1450 rpm, the design flow rate is Q = 0.33 m^3/s, and the design head is H = 8.5 m.

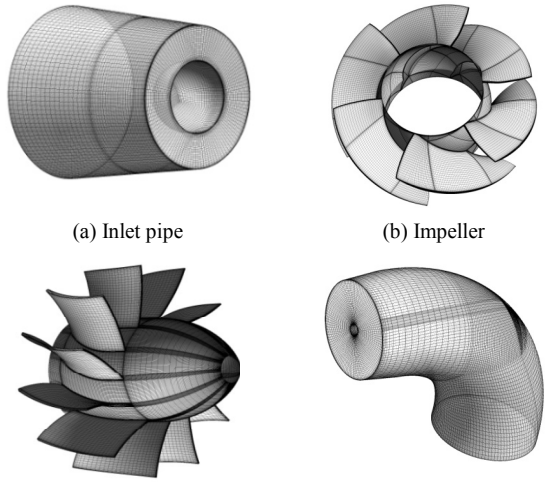

Fig. 2. Grid view of flow components.

2.2 Grid generation

It is known that the convergence of CFD calculations and the accuracy of results are strongly dependent on the quality of the computational grid. For this purpose, the grid generation tool AYSYS ICEM-CFD was employed to create high-quality structured grids with hexahedral elements for the complete axial pump stage. The pump stage was divided into four flow parts for grid generation: inlet pipe, impeller, diffuser and outlet pipe. The grid for each flow component was created separately, and then connected together with general grid interface method. For the impeller and diffuser, a combination of O-grid around the blade and H-grid in the passage was used, in order to take full advantage of O-grid for the ability of good boundary layer resolution. The impeller tip clearance between the blade tip and the casing wall was meshed with 10 nodes in the height direction in the impeller grid, for the purpose of investigation of tip clearance flow. The first grid node from wall was well controlled to ensure y+, the non-dimensional wall distance, below 50 in the whole computational domains, meeting the requirement of the turbulence model chosen in this paper. The total number of grid nodes is 4736636, corresponding to a total number of hexahedral elements of 4496591. The grid view of all flow components is provided in Fig. 2. Through comparing the results with different grid sizes for the pump stage, it is found that the above grid size is fine enough to obtain grid-independent results for the pressure field and also the pump characteristics.

2.3 Numerical methodology

Three-dimensional turbulent flow filed inside the axial pump stage was simulated by using a commercial CFD code ANSYS CFX-14.0. A constant total pressure was specified at the inlet of the computational domain, with flow direction normal to the inlet surface. At the outlet, mass flow rate is

given. Smooth and no-slip condition was imposed on walls. The impeller was defined as a rotating domain, with the other three defined as stationary ones. Three grid interfaces were introduced for the simulation, one was between the inlet pipe and the impeller, one was between the impeller and the diffuser, and the third was between the diffuser and the outlet pipe. Since the impeller was defined in rotating frame of reference, and the rest were defined in stationary frame of reference, multiple frames of reference were involved. The sliding mesh technology was utilized for data transfer through interfaces. For the discretization method, the second order backward Euler scheme was chosen for the time domain, and second order format was used in space and other terms. The interfaces between the impeller and the diffuser, and the inlet pipe and the impeller were set to "transient rotor-stator", in which the relative position between the rotor and stator is updated during each time step. The time step Δt for unsteady calculations was set to 2.2989×10^{-4} s, corresponding to the impeller rotation of 2 degrees at the design rotating speed. The turbulence inside the pump was simulated with the Shear stress transport (SST) turbulence model [18], a combination of a k-ω model applied in the near wall region and a k-ε model employed for the main flow. The SST model is assumed to be able to make a highly accurate prediction on the onset and amount of flow separations under the condition of adverse pressure gradients by including the transport effects into the formulation of the eddy viscosity.

Prior to a transient simulation, a steady flow field was obtained with the interface of "frozen rotor" between the interfaces with multiple frames of reference involved, used as an initial guess for the transient simulation. This "frozen rotor" model transfers the flow flux from one component to the next between different frame of reference while remaining the relative position between the rotor and the stator the same.

3. Results and discussion

All simulation results presented here were obtained for the design operating point for the pump. The total time for the unsteady simulation was set for the impeller to rotate 12 revolutions. The flow field was considered statically periodic generally after 10 impeller revolutions, judged by statistics results and pressure fluctuations on monitor points defined in different domains. Afterwards, 2 more impeller revolutions were calculated further to perform a transient statistics on the flow filed, in which the maximum, minimum, time-average and standard deviation of the selected flow variables (such as pressure, velocity and turbulence kinetic energy) were recorded at each grid node in the computational domains. Note that the grid node belongs to the local frame of reference, i.e., it is rotating with the impeller if located in the impeller domain, and it is stationary if in other domains.

The unsteady pressure at each grid node consists of two parts: the time-averaged part depending on the grid node location, as expressed in Eq. (1), and the fluctuating one changing periodically with the relative position between the rotor and stator during the impeller rotation, as defined in Eq. (2).

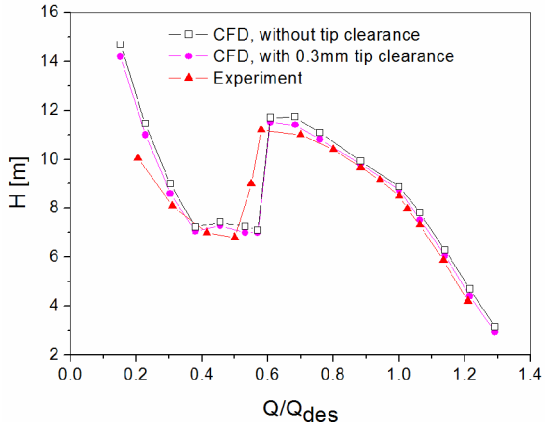

Fig. 3. Head curve of the pump.

$$\bar{p}(node)=\frac{1}{N}\sum_{i=0}^{N-1}p(node,t_0+i\Delta t) \tag{1}$$

$$\tilde{p}(node,t)=p(node,t)-\bar{p}(node)\,. \tag{2}$$

The non-dimensional pressure coefficient Cp_{sdv} in Eq. (3) is defined to determine the magnitude of pressure fluctuation at each grid node, standing for the normalized standard deviation of unsteady pressures:

$$Cp_{sdv}(node)=\frac{\sqrt{\frac{1}{N}\sum_{i=0}^{N-1}\tilde{p}(node,t_0+i\Delta t)^2}}{0.5\rho U_2^2} \tag{3}$$

where N is the sample number during the last 2 impeller revolutions for the statistics, t_0 is the start time for the transient statistics and Δt is the time step used for the simulation.

In addition, in order to examine the tip clearance effects, different sizes of tip clearance have been considered, including zero tip clearance, named as without tip clearance later. This is for the case in which the tip clearance is extremely small. We have calculated the pump with tip clearance = 0.01 mm, and compared the result with the case of tip clearance = 0 (zero tip clearance). The comparison shows that the difference in flow field, including pressure fluctuation and head curve is very small and can be neglected. However, the tip clearance of 0.01 mm is not realistic for an axial pump. Therefore, zero tip clearance is chosen to stand for the case for extremely small tip clearance.

The head curves obtained by CFD simulations and experiment are compared in Fig. 3. For CFD results, two cases are considered: with 0.3 mm tip clearance and without tip clearance. The head in CFD is calculated by the difference of averaged total pressure between the inlet and outlet of the pump divided by the density and gravity acceleration, as expressed in Eq. (4)

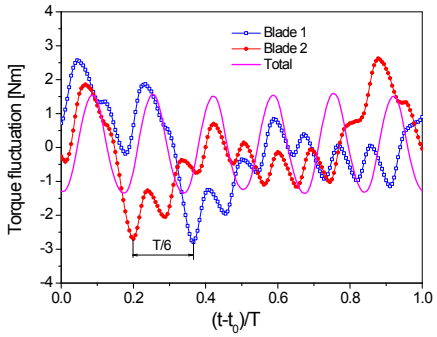

Fig. 4. Torque fluctuation, tip clearance = 0.3 mm.

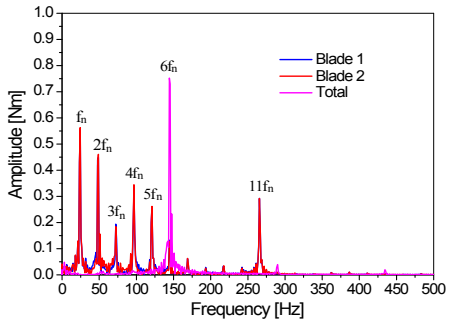

Fig. 5. Frequency spectra of torque fluctuation, tip clearance = 0.3 mm.

$$H = \frac{\overline{P_{tot}^{outlet}} - \overline{P_{tot}^{inlet}}}{\rho g}. \quad (4)$$

It can be seen that the agreement between the CFD result with tip clearance and experiment is generally good, although CFD overestimates slightly the delivery head nearly in the whole flow rate range. For two CFD results, the tip clearance of 0.3 mm causes the head to drop by generally 3%. Furthermore, the hump in the head curve obtained from experiment caused by rotating stalls at part load conditions has also been captured by CFD simulations, but with a small deviation in flow rate where the hump occurs.

Fig. 4 shows the torque fluctuation on two adjacent impeller blades, as well as the total value for all six blades, during one impeller period. Obviously, the torque on one single blade varies strongly with different time according to different relative positions between the selected impeller blade and diffuser vanes. There exists a phase shift of $T/6$ in the distribution curves of torque between blades 1 and 2, due to the physical circumferential position difference (60 deg) between them. In addition, from the frequency spectra of torque fluctuation obtained from Fast Fourier transform (FFT), the highest frequency is the impeller rotating frequency *fn*, followed by some multiple values of *fn*, as well as the diffuser passing frequency Z_d·*fn* (Z_d = 11), as shown in Fig. 5. For the total impeller torque, it exhibits a very good periodicity, dominated by the impeller passing frequency Z_i·*fn* (Z_i = 6).

Fig. 6 shows the pressure fluctuation (only the fluctuating part) during the last two impeller period at some selected monitor points and frequency spectra of pressure fluctuation, with points positions indicated in Fig. 6(a). The monitor points have been placed at half blade height (Span = 0.5), with P1 in the middle of the impeller region, P2 in the axial gap region between the impeller and diffuser, and P3 in the diffuser region near the diffuser vane leading edge. Two cases have been considered: with tip clearance of 0.3 mm and without tip clearance, in order to examine the effect of tip clearance on pressure fluctuation of the main flow. It is observed that at all three monitor points, the pressure fluctuation has been increased by the tip clearance, clearly denoted in Figs. 6(a)-(c). Furthermore, P2 holds the biggest pressure for both cases, due to the point location in the axial gap region where the rotor-stator interaction is generated and therefore is the strongest. The tip clearance has introduced some high harmonics to the frequency spectra of pressure fluctuation in the impeller (Fig. 6(d)), and the impeller frequency *fn* and the diffuser passing frequency Z_d·*fn* are main frequencies for both. At point P2, this phenomenon has been emphasised, and the diffuser passing frequency has dominated. For point P3 in the diffuser, the dominated frequency is the impeller passing frequency Z_i·*fn*, followed by its multiples. Clearly, the amplitude has been augmented by the existence of tip clearance (Fig. 6(f)).

In contrast to plotting fluctuating pressures at selecting points, Fig. 7 illustrates pressure fluctuation contours colored with *Cpsdv* defined in Eq. (3) on different blade-to-blade surfaces for different sizes of tip clearance: 0, 0.3 mm and 0.7 mm, so as to obtain more useful information on pressure fluctuation. In the impeller, *Cpsdv* on the impeller pressure side is bigger than on the suction side at all three blade heights for all three cases, and it increases generally from the impeller Leading edge (LE) to Trailing edge (TE). At the impeller outlet, it can be observed clearly that *Cpsdv* increases generally in the impeller blade height direction from near hub (Span = 0.1) to near shroud (Span = 0.9), this could be due to the fact that the tip clearance affects the flow originally from the blade tip near the impeller shroud.

The quantitative comparison of *Cpsdv* on the impeller blade is plotted in Fig. 8, with the value averaged among all six impeller blades. The tip clearance effect on pressure fluctuation can be easily observed. *Cpsdv* becomes bigger with the increase of tip clearance at all blade heights, and this trend becomes more pronounced from the LE to TE. The highest value of *Cpsdv* on the blade (except the region near the TE and LE) has been increased from about 0.0056 (corresponding to 0.44% of the total head rise of the pump H_{des}) for without tip clearance to 0.0085 (corresponding to 0.67% H_{des}) for with tip clearance of 0.3 mm, and to 0.0093 (corresponding to 0.73% H_{des}) for with tip clearance of 0.7 mm.

For *Cpsdv* in the diffuser region shown in Fig. 7, high pressure fluctuation is located near the diffuser LE, caused by the frequent variation of stagnation point produced by different inflow conditions provided by the upstream impeller during its rotation. High pressure fluctuation is also found near the diffuser vane suction side, with the value of *Cpsdv* higher than

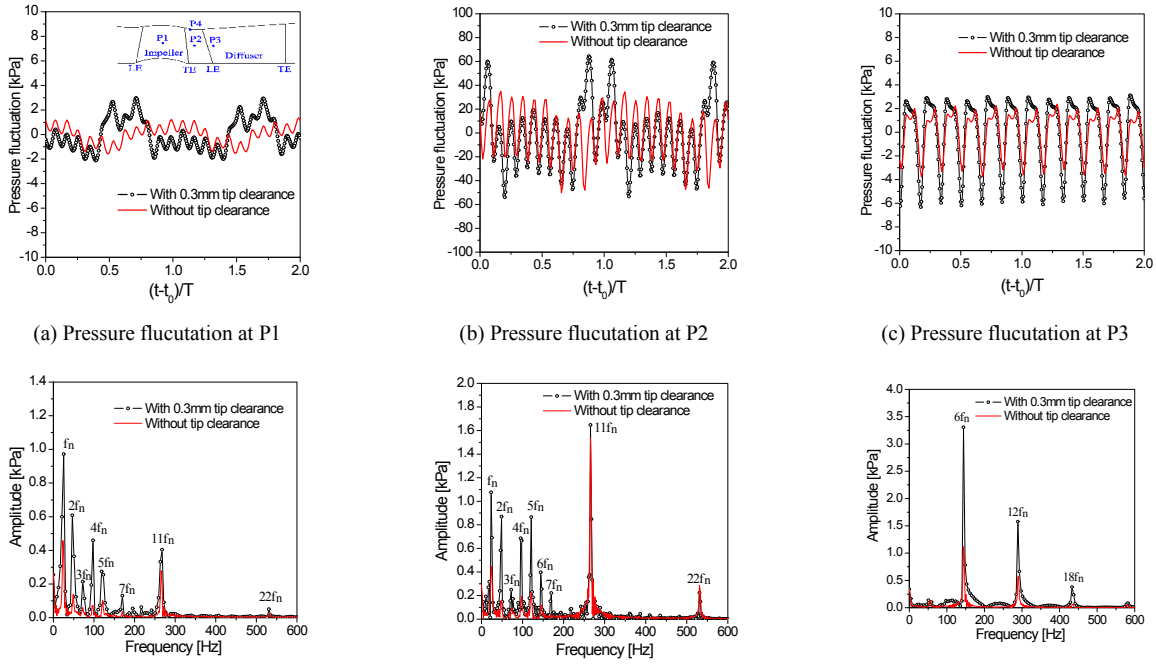

(a) Pressure flucutation at P1 (b) Pressure flucutation at P2 (c) Pressure flucutation at P3

(d) Frequency spectra at P1 (e) Frequency spectra at P2 (f) Frequency spectra at P3

Fig. 6. Pressure fluctuation and frequency spectra at selected monitor points.

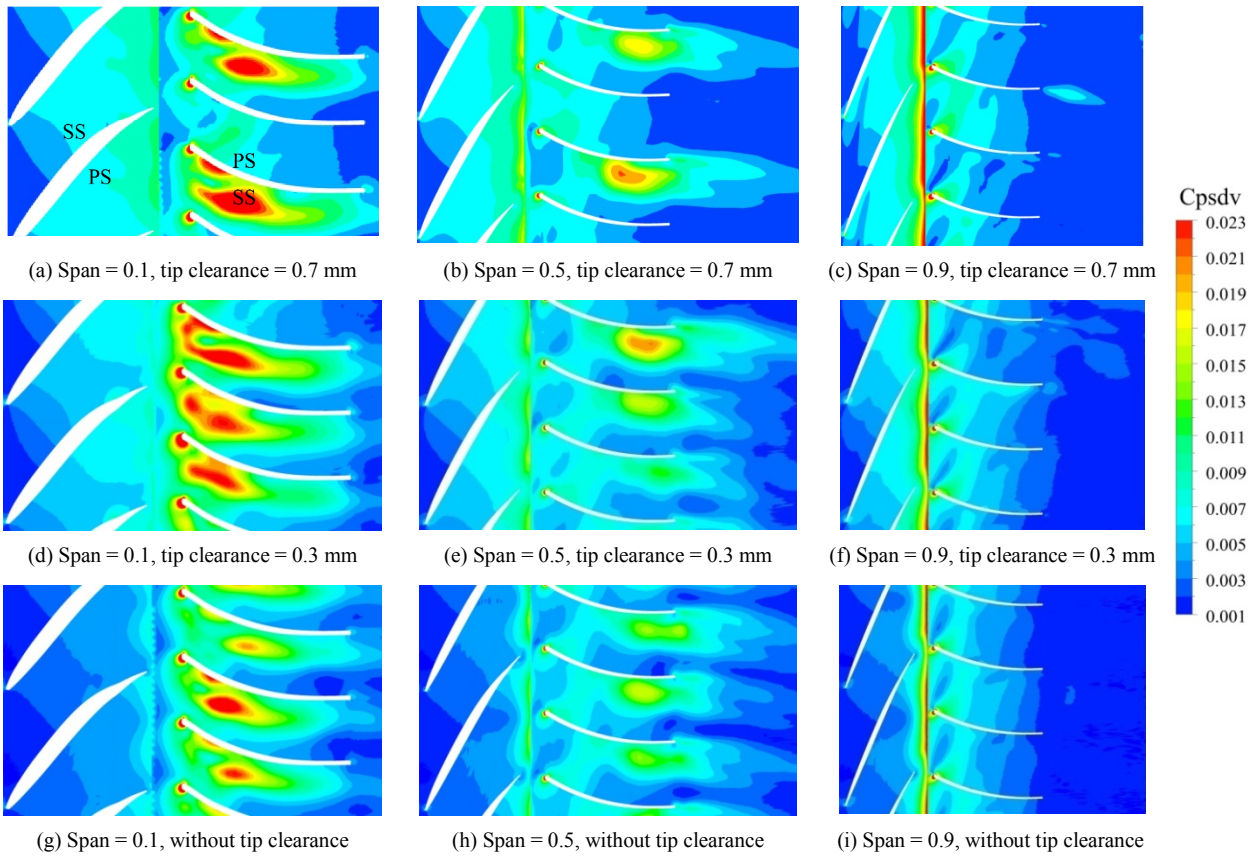

(a) Span = 0.1, tip clearance = 0.7 mm (b) Span = 0.5, tip clearance = 0.7 mm (c) Span = 0.9, tip clearance = 0.7 mm

(d) Span = 0.1, tip clearance = 0.3 mm (e) Span = 0.5, tip clearance = 0.3 mm (f) Span = 0.9, tip clearance = 0.3 mm

(g) Span = 0.1, without tip clearance (h) Span = 0.5, without tip clearance (i) Span = 0.9, without tip clearance

Fig. 7. Comparison of pressure fluctuation contours.

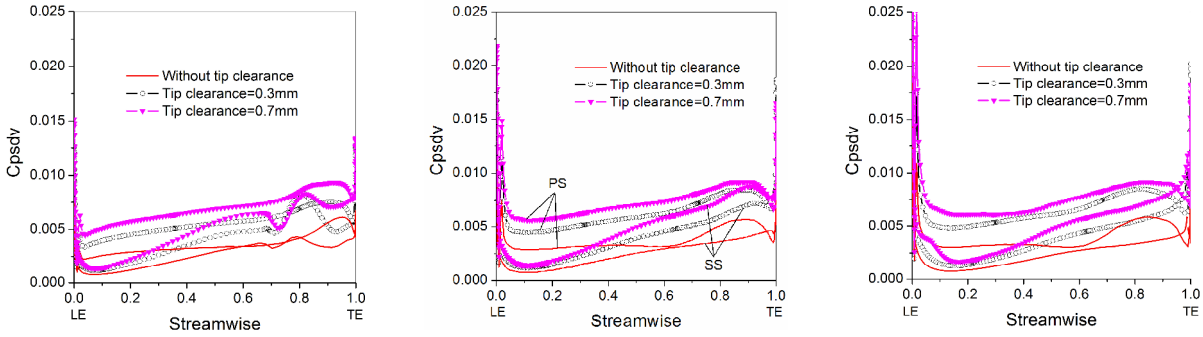

(a) Span = 0.1 (b) Span = 0.5 (c) Span = 0.9

Fig. 8. Comparison of *Cpsdv* on impeller blade.

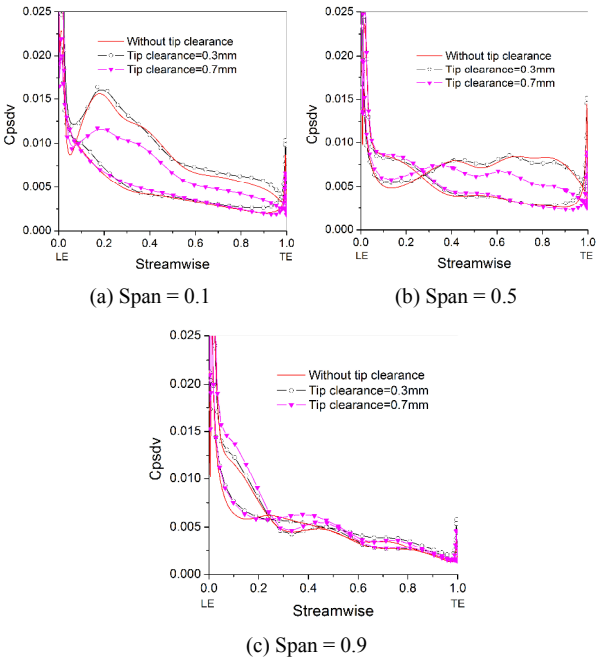

(a) Span = 0.1 (b) Span = 0.5

(c) Span = 0.9

Fig. 9. Comparison of *Cpsdv* on diffuser vane.

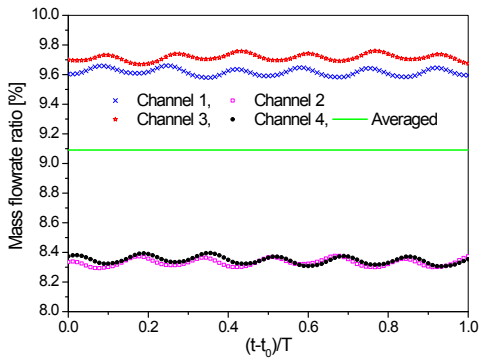

Fig. 10. Mass flow distribution in different diffuser channel, tip clearance = 0.3 mm.

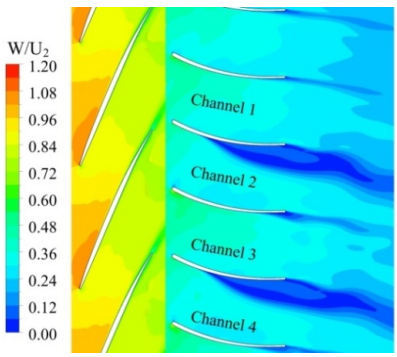

Fig. 11. Relative velocity contours in different diffuser channels, at midspan, tip clearance = 0.3 mm.

0.023, occurring at Span = 0.1. It can be also seen that *Cpsdv* decreases from the hub to shroud for all three sizes of tip clearance, therefore shrinking the tip clearance effect on pressure fluctuation, which can be obtained from the comparison of *Cpsdv* on the diffuser vane surface given in Fig. 9. The increase of tip clearance from zero (without tip clearance) to 0.3 mm does not show evident difference on *Cpsdv*. However, the further increase of tip clearance to 0.7 mm brings a decrease in *Cpsdv* at Span = 0.1 and Span = 0.5. Within the diffuser vane except the region near the TE and LE, the highest value of *Cpsdv* approaches up to 0.016 for tip clearance of zero and 0.3 mm, and 0.012 for tip clearance of 0.7 mm at Span = 0.1, around 0.009 at Span = 0.5, and about 0.013 at Span = 0.9, higher than on the impeller blade.

Fig. 10 illustrates the mass flow rate as function of time in four adjacent diffuser channels during one impeller rotation period. The influence of impeller blades is very evident, which can be easily indentified by six (Z_r = 6) pairs of peaks and valleys in the distribution, shown in Fig. 10. It is also found that the mass flow rate is not uniform among different diffuser channels, and Chanells 1 and 3 hold about 16% higher value than the other two channels, due to the flow non-uniformity in the circumferential direction which is quite clear in Fig. 11. In addition, the fluctuation of mass flow rate in a single diffuser channel is about 1.5% for all shown diffuser channels.

Fig. 12 shows the streamlines in meridional plane of the

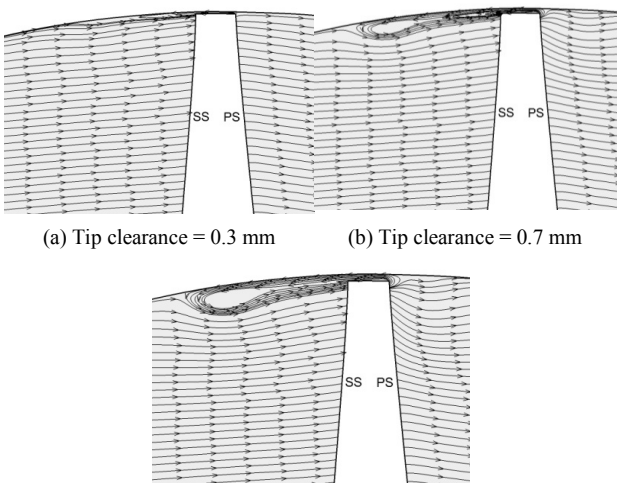

(a) Tip clearance = 0.3 mm (b) Tip clearance = 0.7 mm

(c) Tip clearance = 1.0 mm

Fig. 12. Streamlines at one timestep in meridional plane at different tip clearances.

impeller at different tip clearances, with SS and PS denoting the suction surface and pressure surface of the impeller blade, respectively. Obviously, the flow pattern of tip vortex strongly depends on the size of tip clearance. At tip clearance of 0.3 mm in Fig. 12(a), the flow near the tip clearance flows from PS to SS through the tip clearance, forming a small region with vortex on the suction side near the impeller shroud. With the increase of tip clearance to 0.7 mm shown in Fig. 12(b), the tip vortex becomes stronger and more evident, interacting with the main flow near the shroud and producing a local back flow in that region. In Fig. 12(c) for tip clearance of 1.0 mm, the flow pattern mentioned becomes more evident, and it influences strongly the main flow near the tip on the suction side.

In order to investigate the influence of grid size on the result of pressure fluctuation for the pump, the selected grid size has been doubled, with a scaling factor of 1.26 in grid element number in each grid direction, to generate refined grid for the CFD simulation for the case of tip clearance of 0.3 mm. According to the comparison of unsteady pressure fluctuation in Fig. 13 obtained from two grid sizes at pre-defined monitoring points, such as P4 indicated in the subfigure which is positioned near the impeller blade trailing edge and near the tip clearance (at Span = 0.995), it is clear that doubling the grid size does not have evident influence on the pressure fluctuation. Therefore, the selected grid size is assumed to be fine enough to get grid independent results for the pump stage.

4. Conclusions

The tip clearance effect on pressure fluctuations in an axial flow water pump has been investigated by CFD method through the comparison between with tip clearance of 0.3 mm and without tip clearance, and the pressure fluctuations inside the whole pump have been determined both quantitatively and qualitatively based on the standard deviation of unsteady pressures in the last two impeller revolutions. Main conclusions can be drawn as follows:

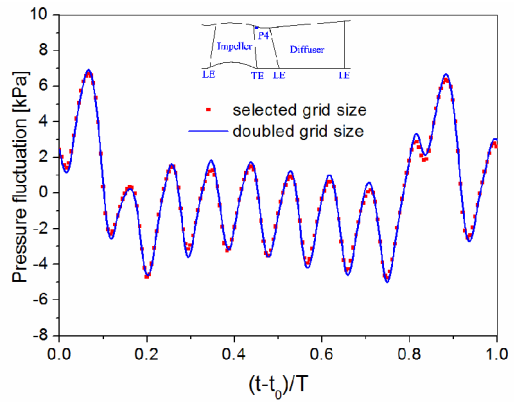

Fig. 13. Pressure fluctuations at monitor point P4 for different grid sizes, tip clearance = 0.3 mm.

(1) The chosen CFD method is capable of capturing the hump in the head curve, but with a small deviation in the flow rate where it occurs when compared with experimental results.

(2) The tip clearance introduces some lower multiples of the rotation frequency of the pump to the frequency spectra of the unsteady pressure in the impeller, but nearly no influence on that in the diffuser.

(3) The tip clearance has magnified greatly the pressure fluctuation in the whole impeller region, and the highest value of *Cpsdv* on the impeller blade has been increased by the tip clearance. The highest standard deviation of unsteady pressure on the impeller blade (except the region near the LE and TE) has been magnified from 0.44% of the total head rise H_{des} of the pump for zero tip clearance to 0.67%H_{des} for tip clearance of 0.3 mm and to 0.73%H_{des} for tip clearance of 0.7 mm.

(4) The increase of tip clearance does not result in an increase of pressure fluctuation in the diffuser region. In addition, the pressure fluctuation on the diffuser vane is higher than on the impeller, and the pressure fluctuation distribution in the span direction is more uniform in the impeller than in the diffuser.

(5) The flow pattern of tip vortex strongly depends on the size of tip clearance, and it influences strongly the main flow on the impeller suction side near the shroud with the increase of tip clearance.

Acknowledgment

This research was supported by the National Natural Science Foundation of China (Grant Nos. 51339005, 51379174, 51479166, and 51479167) and the Scientific Research Foundation for the Returned Overseas Chinese Scholars, State Education Ministry.

Nomenclature

Cpsdv : Pressure fluctuation coefficient

D : Diameter
fn : Impeller design frequency
g : Acceleration due to gravity
H : Delivery head
LE : Leading edge
n : Rotating speed
p : Static pressure
p_{tot} : Total pressure
PS : Pressure surface
Q : Volume flow rate
SS : Suction surface
t : Time
T : Pump period
TE : Trailing edge
U : Circumferential velocity
W : Relative velocity
Z : Number of blades
ρ : Density of water
Δt : Time step

Subscripts

2 : Impeller outlet
i : Impeller
d : Diffuser
des : Design
sdv : Standard deviation

Superscripts

– : Phase-averaged, time-averaged
~ : Fluctuating

References

[1] H. X. Wu, R. L. Miorini and J. Katz, Measurements of the tip leakage vortex structures and turbulence in the meridional plane of an axial water-jet pump, *Experiments in Fluids*, 50 (4) (2011) 989-1003.

[2] W. C. Zierke, W. A. Straka and P. D. Taylor, Experimental investigation of the flow through an axial-flow pump, *Journal of Fluids Engineering*, 117 (3) (1995) 485-490.

[3] W. C. Zierke, K. J. Farrell and W. A. Straka, Measurements of the tip clearance flow for a high-Reynolds-number axial flow rotor, *ASME Journal of Tubomachinery*, 117 (4) (1995) 522-532.

[4] D. S. Zhang et al., Numerical investigation of blade dynamic characteristics in an axial flow pump, *Thermal Science*, 17 (5) (2013) 1511-1514.

[5] D. S. Zhang et al., Study on tip leakage vortex in an axial flow pump based on modified shear stress transport k-ω turbulence model, *Thermal Science*, 17 (5) (2013) 1551-1555.

[6] R. Dong, S. Chu and J. Katz, Effect of modification to tongue and impeller geometry on unsteady flow, pressure fluctuations, and noise in a centrifugal pump, *Journal of Turbomachinery*, 119 (3) (1997) 506-515.

[7] K. A. Kaupert and T. Staubli, The unsteady pressure field in a high specific speed centrifugal pump impeller-part 1: influence of the volute, *Journal of Fluids Engineering*, 121 (3) (1999) 621-626.

[8] Q. R. Si, J. P. Yuan and S. Q. Yuan, Numerical investigation of pressure fluctuation in centrifugal pump volute based on SAS model and experimental validation, *Advances in Mechanical Engineering*, 2014 (2014) Article ID 972081, 12.

[9] W. Qin and H. Tsukamoto, Theoretical study of pressure fluctuations downstream of a diffuser pump impeller-part 1: fundamental analysis on rotor-stator interaction, *Journal of Fluids Engineering*, 119 (3) (1997) 647-652.

[10] H. Wang and H. Tsukamoto, Fundamental analysis on rotor stator interaction in a diffuser pump by vortex method, *Journal of Fluids Engineering*, 123 (4) (2001) 737-747.

[11] H. Wang and H. Tsukamoto, Experimental and numerical study of unsteady flow in a diffuser pump at off-design conditions, *Journal of Fluids Engineering*, 125 (5) (2003) 767-778.

[12] F. Shi and H. Tsukamoto, Numerical study of pressure fluctuations caused by impeller-diffuser interaction in a diffuser pump stage, *Journal of Fluids Engineering,* 123 (3) (2001) 466-474.

[13] J. Feng, F.-K. Benra and H. J. Dohmen, Numerical investigation on pressure fluctuations for different configurations of vaned diffuser pumps, *International Journal of Rotating Machinery*, 2007 (2007) Article ID:34752, 10.

[14] D. Zhang et al., Unsteady flow analysis and experimental investigation of axial-flow pump, *Journal of Hydrodynamics*, 22 (1) (2010) 35-43.

[15] Z. J. Shuai et al., Numerical study on the characteristics of pressure fluctuations in an axial-flow water pump, *Advances in Mechanical Engineering*, 2014 (2014) Article ID 565061, 7.

[16] C. Kang et al., Influence of stator vane number on performance of the axial-flow pump, *Journal of Mechanical Science and Technology*, 29 (5) (2015) 2025-2034.

[17] B. Ji, X. W. Luo and Y. L. Wu, Unsteady cavitation characteristics and alleviation of pressure fluctuations around marine propellers with different skew angles, *Journal of Mechanical Science and Technology*, 28 (4) (2014) 1339-1348.

[18] F. R. Menter, Two-equation eddy-viscosity turbulence models for engineering applications, *AIAA-Journal*, 32 (8) (1994) 1598-1605.

Jianjun Feng received his Ph.D. degree from University of Duisburg-Essen in Germany in 2008. Afterwards, he worked as a post-doctor in the same university. Since late 2011, he has been a full professor in Xi'an University of Technology in China. His main scientific interests are rotor-stator interactions including CFD simulations and flow measurements by PIV and LDV and optimization design of turbo-machines.